Optical Review (2021) 28:8–17
https://doi.org/10.1007/s10043-020-00628-2

REGULAR PAPER

Design of an omnidirectional gaze optical imaging system with ultrahigh resolution

Shuai Liu[1] · Chunyu Liu[1] · Guang Jin[1] · tiancong Wang[1]

Received: 21 November 2019 / Accepted: 11 November 2020 / Published online: 2 January 2021

Abstract
In this study, we discuss a new method to optimize the design of an omnidirectional gaze optical imaging system with ultrahigh resolution and long focus. An aspheric diffractive optical element is used in the optical system to offer more freedom, simplify the structure, and decrease the chromatic aberration. Owing to large image sensor arrays, the omnidirectional gaze photoelectric imaging system is capable of overcoming the shortcoming of low peripheral resolution. This has led to an increased usage of this system in military applications. Here, we describe a six-piece optical system installed on an 80 MPx full-frame CCD with 10,320 × 7752 pixels, 5.2 μm pixel size, 200° × 360° field of view, and an effective focal length of 11.6 mm. The difficulties in designing an ultrahigh-resolution fish-eye lens have been discussed and addressed. Furthermore, system performance evaluation, tolerance analysis, and image distortion calibration were also performed.

Keywords Omnidirectional gaze image · Optical design · High resolution · Aspheric diffractive element · Image calibration

1 Introduction

An omnidirectional gaze optical imaging system is a bionic equipment that mimics the fish gaze in a manner similar hemisphere scene in the water. The imaging model of incident rays traveling inside a fisheye is shown in Fig. 1. As a well-known spherical imaging model [1], the omnidirectional gaze optical system transforms from a three-dimensional (3D) omnidirectional hemisphere or hyper hemisphere globe field of view (FOV) to a two-dimensional (2D) spherical image plane perpendicular to the optical axis, as shown in Fig. 2. Owing to the large FOV, the system can access the target in real-time in the hemispherical space; however, the imaging edge resolution is always relatively low. Further, many important applications for full-field imaging require a higher resolution; therefore, it is essential to the study the omnidirectional gaze optical system with an ultrahigh resolution.

The growing popularity of the wide-angle optical system in electronic applications have led to an increasing interest in fisheye lens [2–6]. Mizuguchi designed the first compact fisheye lens using minimum eight lens elements [7, 8]. The first megapixel fisheye lens was produced by Fujinon. A panomorph lens has a 360° coverage with enhanced resolution-adjusting pixel density in predefined zones of interest [9, 10]. A foveated fisheye lens is defined by an angle-variant distortion model such as the space-variant resolution of the human retina [11, 12]. However, none of these studies reported the design of a fisheye lens with a large image sensor array.

In the conventional pinhole optical imaging systems shown in Fig. 3a, the target object at infinity is similar to the image, thus following Gaussian optics. The relationship between the image height R and the incident angle θ can be expressed as Eq. (1), where f' is the focal length of the lens.

$$R = f' \tan\theta. \tag{1}$$

The conventional FOV equation does not apply to the fisheye lens when the $|\theta| \geq 90°$. Therefore, the fisheye lens must have different theories from that of Gaussian optics, as shown in Fig. 3b by artificially introducing barrel distortion to compress the image light out of the range of Gaussian optics. Here, R' is the height of the image surface.

✉ Shuai Liu
568296405@qq.com

✉ Chunyu Liu
mmliucy@163.com

[1] Changchun Institute of Optics, Fine Mechanics and Physics, Chinese Academy of Sciences, Changchun 130033, China

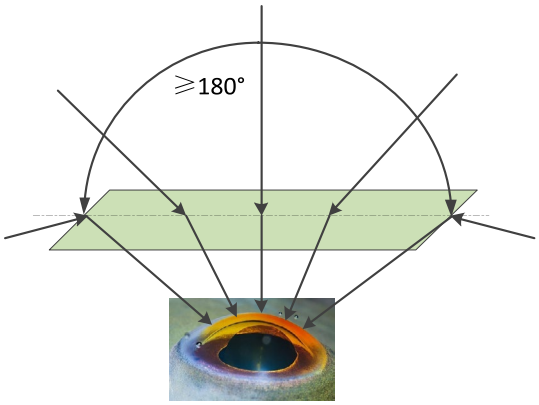

Fig. 1 Fisheye bionic model

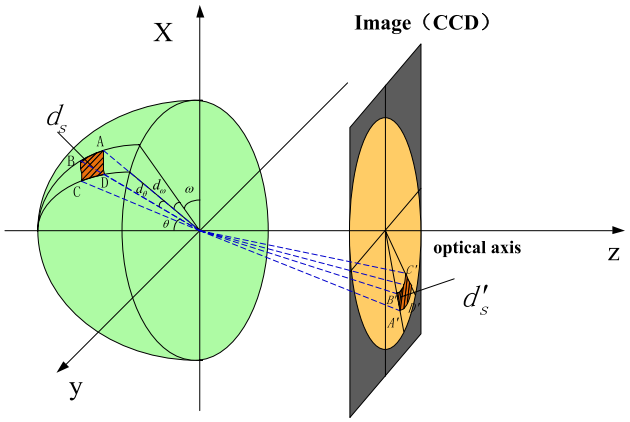

Fig. 2 Object-image relationship of fisheye lens

In this paper, we elucidate one of the extraordinarily consequential discussions in the design of omnidirectional gaze optical system with ultrahigh resolution. The omnidirectional gaze optical system contains two aspheric surfaces and an aspheric diffractive optical element (ADOE) surface, which would offer more freedom and reduce the number of lens. The total length of the fisheye lens is 73 mm and the maximum diameter is 74 mm. The modulation transfer functions (MTFs) of the center and marginal fields are close to 0.6 and 0.3, respectively, at 100 lp/mm of Nyquist frequency in the full range of visible-light wavelength. Owing to the presence of the ADOE, the chromatic aberration resembles an airy disk and the distortion is less than 0.5%.

2 Relative illumination and off-axis aberration of the ultrahigh resolution system

2.1 Relative illumination

The relative illumination will decay according to the $\cos^4 \theta'$ law and decline to 6.25% with an exit angle of 60° to obtain a larger design of field. We selected the well-known inverted telephoto objective lens of first order, shown in Fig. 4, which consists of a front–back optical group with focal powers φ_1 and φ_2. The front group of the lens provides ultra-wide incident rays to the optical system using a highly negative power that can effectively improve the relative illumination.

Fisheye projection functions are designed to project an entire hemispherical image onto a flat image surface along with introducing large barrel distortion. According to the panoramic system, the essential fisheye equidistance projection schemes are considered in this design. Based on Eq. (2), the image height (R') increases with the object incident angle (θ); hence, we can improve the relative illumination by bending the marginal rays to the center of the image and directly calculating the object space coordinates from the image.

$$R' = f'\theta. \tag{2}$$

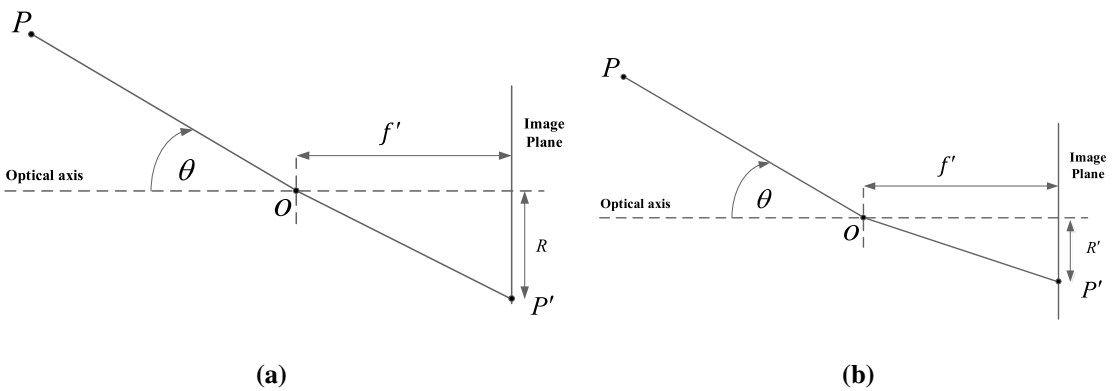

Fig. 3 **a** Rectilinear (pinhole camera) imaging model and **b** fisheye imaging model

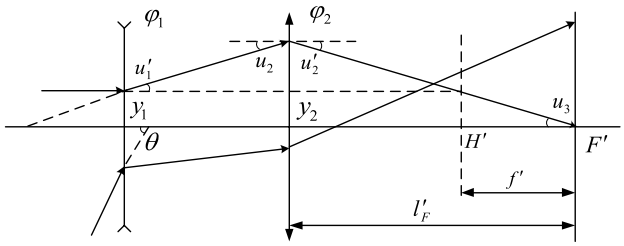

Fig. 4 Ray diagram of the inverted telephoto lens

Certain optical systems, such as a fisheye lens with a large F/# or large field angles, may have significant entrance pupil aberration. The primary part is represented as follows [13]:

$$w_p = \frac{1}{8}S_{\mathrm{I}p}(\eta^2+\zeta^2)^2 + \frac{1}{2}S_{\mathrm{II}p}(\eta y+\zeta z)(\eta^2+\zeta^2) + \frac{1}{2}S_{\mathrm{III}p}(\eta y+\zeta z)^2 + \frac{1}{4}(S_{\mathrm{III}p}+S_{\mathrm{IV}p})(\eta^2+\zeta^2)(y^2+z^2) + \frac{1}{2}S_{Vp}(\eta y+\zeta z)(y^2+z^2), \tag{3}$$

where $S_{\mathrm{I}p}, S_{\mathrm{II}p}, S_{\mathrm{III}p}, S_{\mathrm{IV}p}, S_{Vp}$ are stop spherical aberration, stop coma aberration, stop astigmatism aberration, stop field-curve aberration, and stop distortion aberration, respectively. Further, η, ζ are the object coordinates; y, z are the coordinates of the stop plane. We calculated the η, ζ coordinates from Eq. (3) to obtain the difference between the real entrance pupil and the ideal stop image, which is called the vertical-axis geometry aberration of the stop. Only considering the meridian plane with $\zeta = 0$ yields the results shown in Eqs. (4) and (5):

$$\left(\frac{\partial w_p}{\partial \eta}\right)_{\zeta=0} = \frac{1}{2}S_{\mathrm{I}p}\eta^3 + \frac{3}{2}S_{\mathrm{II}p}\eta^2 y + S_{\mathrm{III}p}\eta y^2 + \frac{1}{2}(S_{\mathrm{III}p}+S_{\mathrm{IV}p})\eta(y^2+z^2) + \frac{1}{2}S_{Vp}(y^2+z^2)y, \tag{4}$$

$$\left(\frac{\partial w_p}{\partial \zeta}\right)_{\zeta=0} = \frac{1}{2}S_{\mathrm{II}p}\eta^2 z + S_{\mathrm{III}p}\eta yz + \frac{1}{2}S_{Vp}(y^2+z^2)z. \tag{5}$$

According to these equations, stop coma aberration $S_{\mathrm{II}p}$ can enlarge the area of the off-axis beam exit pupil such that the cross-sectional area of the off-axis beam is larger than the on-axis beam at the entrance pupil plane. Therefore, the real imaging relative illumination can be expressed as Eq. (6):

$$E_{\mathrm{M}}' = E'\frac{S_\theta}{S_o}\cos^4\theta', \tag{6}$$

where S_θ and S_o are the cross-sectional areas of the off- and on-axes beams, respectively. Further, E_{M}' is the off-axis illumination, and E' is the on-axis illumination. The stop coma aberration vignette enables higher relative illumination.

2.2 Off-axis aberration

2.2.1 Field-curve

The fundamental parameters of inverted telephoto objective lens can be defined by Eq. (10), which describes the relationship between the optical power and various parameters of the fisheye lens. These parameters are inferred from the refraction law and the transition equalities as follows in Eqs. 7, 8, 9.

$$\tan u_1' = y_1\varphi_1 = \tan u_2, \tag{7}$$

$$\tan u_2' = \tan u_2 + y_2\varphi_2, \tag{8}$$

$$\tan u_3 = \frac{y_2}{l_F'} = \frac{y_1}{f'} = \tan u_2', \tag{9}$$

$$\varphi = \frac{1}{f'} = \frac{1}{y_1}\sum_{i=1}^{n} y_i\varphi_i, \tag{10}$$

where φ_i is the optical power of the respective elements, y_i is the incident height of the co-boundary rays at each surface, u_i is the incident angle of the respective surfaces, f' is the effective focal length, and l_{F}' is the back focal length.

The Seidel wavefront polynomial term of Petzval field curvature is shown in Eq. (11).

$$W_{220} = \frac{1}{4}S_{\mathrm{IV}} = -\left(\frac{L^2}{4}\right)\sum_{i=1}^{n}\rho_i\Delta\left(\frac{1}{n_i}\right) \tag{11}$$

where W_{220} is the Petzval field curvature wavefront coefficient, S_{IV} is first-order field curvature Seidel coefficient, L is the system Lagrange invariant, ρ_i is the curvature of the respective elements, and n_i is the refractive index. Because L is a constant, the Petzval wavefront coefficient mainly depends on the surface curvature and the refractive index of the material. Therefore, to make the imaging plane smoother to match with the plane image sensor, summation in Eq. (12) should be minimized as far as possible.

$$\sum_{i=1}^{n}\rho_i\Delta\left(\frac{1}{n_i}\right) = \rho_1\left(\frac{1}{n_1}-1\right) + \rho_2\left(1-\frac{1}{n_1}\right) + \cdots + \rho_{i-1}\left(\frac{1}{n_i}-1\right) + \rho_i\left(1-\frac{1}{n_1}\right) = \sum_{i=1}^{n}\frac{\varphi_i}{n_i}. \tag{12}$$

Here, $\phi_i = (n_i - 1)(\rho_{i-1} - \rho_i)$ is the common equation for a thin-lens optical power.

2.2.2 Chromatic aberration

The chromatic aberration in the first-order structure can be eliminated using Eq. (13).

$$\sum C_{\mathrm{I}} = y_1^2 \frac{\phi_1}{\nu_1} + y_2^2 \frac{\phi_2}{\nu_2} = 0, \tag{13}$$

where $\phi_1\phi_2$ is the power of the front-back optical group, as expressed in Eq. (14), and its summation gives the total power:

$$\phi = \phi_1 + \phi_2. \tag{14}$$

3 Optical design

Based on the correction theories for the relative illumination and off-axis aberration discussed in Sect. 2, the design and optimization of the fisheye lens with an ultrahigh resolution is discussed in this section.

3.1 Design specifications

To realize real-time detection of hemispherical space with an ultrahigh resolution image, we used a full-frame CCD with 10,320×7752 active pixels and 5.2 μm^2 pixel size. The active focal length of the optical system can be calculated by Eq. (15), the limit of f-theta distortion should be less than 1%, and the MTF value at a Nyquist frequency of 96 lp/mm should be greater than 0.1 for the clear detection of the fisheye lens.

$$f' = \frac{r}{\theta} \tag{15}$$

On the one hand, the fisheye lens should have a large relative aperture, resulting in high optical diffraction limit resolution and ensuring sufficient illumination on the fringe of the image to catch more light in the dim environment.

On the other hand, with the increase in the relative aperture and FOV, the rays are bent strongly, the focal length increases with the increase in the width of the CCD. Moreover, the off-axis and high-order aberrations increase rapidly. Therefore, to ensure excellent performance of the fisheye lens requires many lens, high image resolution, and a complex design. However, this will complicate the manufacturing process and its operation, but also the low transmission. To simplify the structure, an ADOE surface is used instead of a spherical surface to offer freedom of design. Moreover, the effort of wavefront phase modulation to balance off-axis aberration and special negative dispersion to correct the chromatic aberration.

We even considered the ASP surface model, which uses only the even powers of the radial coordinate to describe the asphericity. Therefore, the surface sag is given by Eq. (16).

$$z = \frac{ch^2}{1 + \sqrt{1 - (1+k)c^2h^2}} + \sum_{i=1}^{8} \alpha_i h^{2i} \tag{16}$$

The rotationally symmetric diffractive optical element (DOE) surface adds phase to the ray according to the following polynomial expansion Eq. (17):

$$\psi = M \sum_{j=1}^{N} A_j \rho^{2j}, \tag{17}$$

where z is the corresponding vertical distance; h is the radial distance from the aspheric axis; $\alpha_1 \sim \alpha_8$ are the high-order polynomial coefficients; c is the reciprocal of the base radius; k is the conic constant of the surface; N is the number of polynomial coefficients in the series; A_j is the diffractive coefficient of ρ, which is the normalized radial aperture coordinate; and M is the diffraction order. The focal power of ADOE ψ mainly depends on A_1 and the curvature distribution. The transmission ability of the optical system to different frequencies of the target can be reflected by the MTF value, which gradually decreases with increasing frequency. Because the resolution threshold of the CCD is 0.1, we suggest that the image clearly when the MTF value is above 0.1 at the Nyquist frequency [14]. In military applications, the *F*-theta distortion is required to be under 1% and the relative illumination should be above 50% for accurate observations. Table 1 shows the specifications of the optical system.

Table 1 Design specifications

Parameter	Value
CCD optical size	53.6 mm×40.3 mm
Pixel size	5.2 μm×5.2 μm
Resolution	10,320×7752
Imaging diameter	40.3 mm
Wavelength band	486–656 nm
Field of view/(°)	200°×360°
F/#	≤ 4
Number of lens elements	6
Focal length	11.6 mm
Image quality	MTF > 10%(96 lp/mm)
F-Theta distortion	≤ 1%

3.2 Optimization scheme

According to the part 2 and design specifications, a symmetric fisheye lens with a focal length of 10.33 mm and an imaging radius of 14.13 mm was considered as the first-order configuration in the design of the omnidirectional gaze optical imaging system with ultrahigh resolution [15]. A schematic of this configuration is shown in Fig. 5. The maximum angle is 90°, while the optical axis is plotted along the horizontal and the FOV corresponds to a vertical circular plane.

The ultrahigh-resolution fisheye lens is based on this configuration and is optimized through ray aiming using ZEMAX. In the optimization, the center location and the direction of the entrance pupil will change with the incident angle, which can improve the relative illumination using the stop coma aberration and the effective focal length (EFFL). The rage of image is taken as the basic target for the configuration optimization of the fisheye lens, the MTF, and *F*-theta distortion, and the lateral color aberration is set as the primary principle for the merit function. In addition, the fisheye lens is designed to be symmetrical with a co-axial surface; therefore, only half of the rotational angles, from 0° to 100°, should be optimized.

First, a focal scale was generated and the EFFL of the lens was maintained at 11.6 mm. Then, based on the relationship between the thickness and the semi-diameter of the elements to limit the variables within an appropriate range, the distortion was controlled by the real ray height at the image surface, as shown in Table 2.

The MTF is an important indicator for an imaging optical system; therefore, there are different requirements for all fields at 100 lp/mm and 50 lp/mm, and the weight should be more with the low MTF. The ASP surface and the ADOE phase coefficients may be considered up to the eighth-order term. Moreover, the back surface of the first element should not form a super hemisphere. Before the system can be produced, the radius, thickness, and glass material of the lens should be standardized to meet the industry standards.

4 Design result

4.1 Optical structure parameters

After a series of analysis and optimization, we obtained a compact and high-resolution fisheye lens, whose structure and 3D plot are shown in Figs. 6 and 7, respectively. The EFFL was 11.6 mm in the visible spectrum and F# was 4. The field of the lens was 200° × 360° and the real image diameter—with maximum barrel distortion of − 0.25%—was 40.3 mm. Further, the effective resolution of the lens was 60 MPx. The first negative meniscus, convex toward the object, had a maximum diameter of 74 mm, and the total tracking length was only 73 mm, while the back focal length reached 19.3 mm.

The fisheye lens contains six optical elements. Further, it contains two ASP surfaces and an ADOE as the cemented surface. The diffractive coefficients are as follows: $A_1 = -7.183 \times 10^4$, $A_2 = -5.531 \times 10^5$, $A_3 = 1.471 \times 10^8$, and $A_4 = 8.073 \times 10^9$. The diffraction order, effective diffractive radius, and normalization radius are 1, 9.83 mm, and

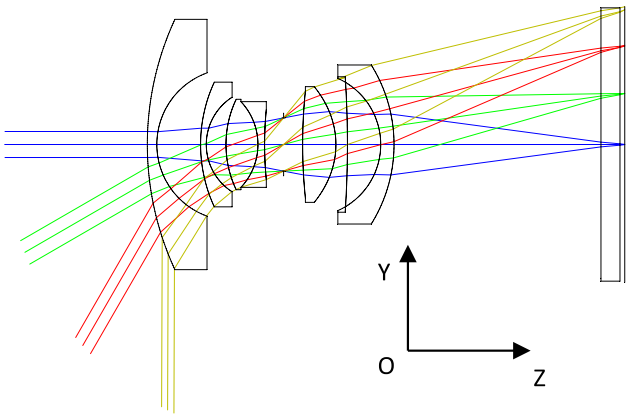

Fig. 5 First-order configuration

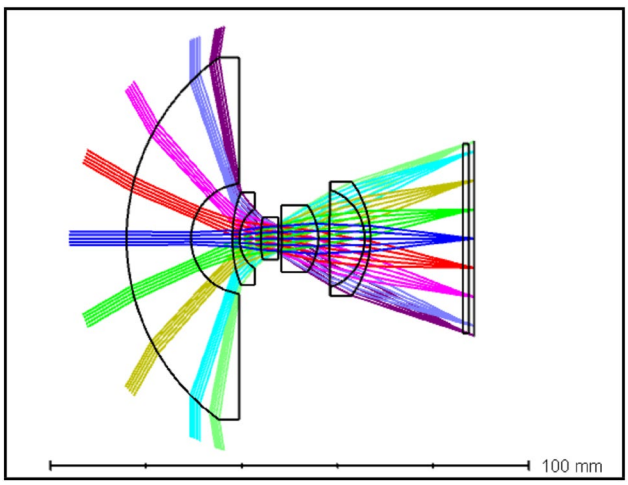

Fig. 6 Layout of the ultrahigh resolution fisheye lens

Table 2 Ideal imaging height

FOV (°)	100	90	70	50	30	0
Height (mm)	20.246	18.221	14.172	10.123	6.074	0

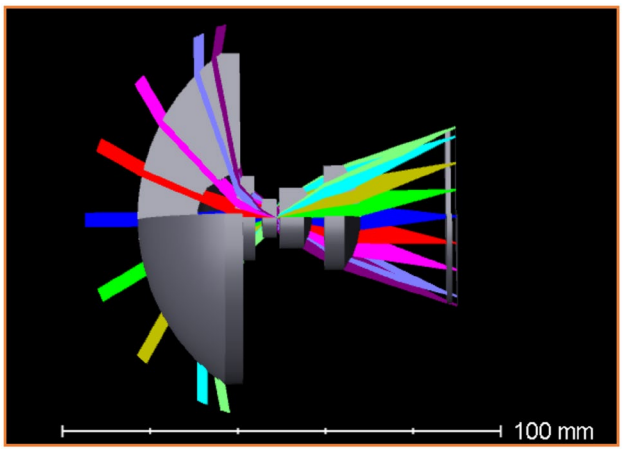

Fig. 7 3D layout of the ultrahigh resolution fisheye lens (3/4th section)

90 mm, respectively. The phase plot is shown in Fig. 8. The periods increase with the diffractive radius, the most line frequency is 29.46 Periods/mm, so the minimum width 33.94 µm in one period, which is available to be realized by the process of diamond cutting, that the period precision of the minimum width is better than 5 µm [16]. It has a maximum diffraction efficiency at a pitch of 33.94 µm, and the calculation formula is as follows [17]:

$$H = \frac{N}{N-1}\frac{\lambda}{n_t(\lambda) - n_i(\lambda)} \tag{18}$$

$$\eta_m = \sin c^2\left\{ m - \frac{H}{\lambda}\left[n_i(\lambda)\cos(\theta_i) - n_t(\lambda)\cos(\theta_t)\right]\right\} \tag{19}$$

$$\bar{\eta}_m = \frac{1}{\lambda_{\max} - \lambda_{\min}} \int_{\lambda_{\min}}^{\lambda_{\max}} \eta_m d_\lambda, \tag{20}$$

where H is the microstructure height of ADOE, η_m is the diffraction efficiency of the oblique incidence of light, $\bar{\eta}_m$ is the diffraction efficiency of a wide spectrum. The incident and exit angles of the ADOE were 51.464° and 42.674°, respectively. The light incident medium was N-PSK57 and the refractive index $n_i(\lambda)$ was 1.592. Further, the light-emitting medium was SF57 and the refractive index $n_t(\lambda)$ was 1.846. The central wavelength, $\lambda_{\max}$, and $\lambda_{\min}$ of the system were 587, 656, and 486 nm, respectively. The line frequency N of the ADOE was 29.46 Periods/mm. We substituted these parameters in Eqs. (18)–(20) and obtained a diffraction efficiency of 92% at a pitch of 33.94 µm.

Tables 3 and 4 list the detailed lens data and the coefficients of the ASP surface. An optical low-pass filter of 1.6 mm was placed before the imaging plane.

4.2 Performance evaluation

Since the selected pixel size of the CCD was 5.2 µm, the corresponding Nyquist frequency (NF) was about 96 lp/mm. The modulation transfer function should be greater than 0.1 as per the design specifications. To avoid the oversampling risk, we should test our system using a sensor with a slightly larger NF. As shown in Fig. 9, the MTFs of all fields were above 0.3 at 100 lp/mm, which is close to the diffractive limitation. Further, the astigmatism of the system was corrected successfully and the gap between tangential and sagittal MTFs was small. Therefore, the fisheye lens of ultrahigh-resolution has a good image performance.

Figure 10 shows the field curvature and f-theta distortion curve. The first-order and the higher-order curvature

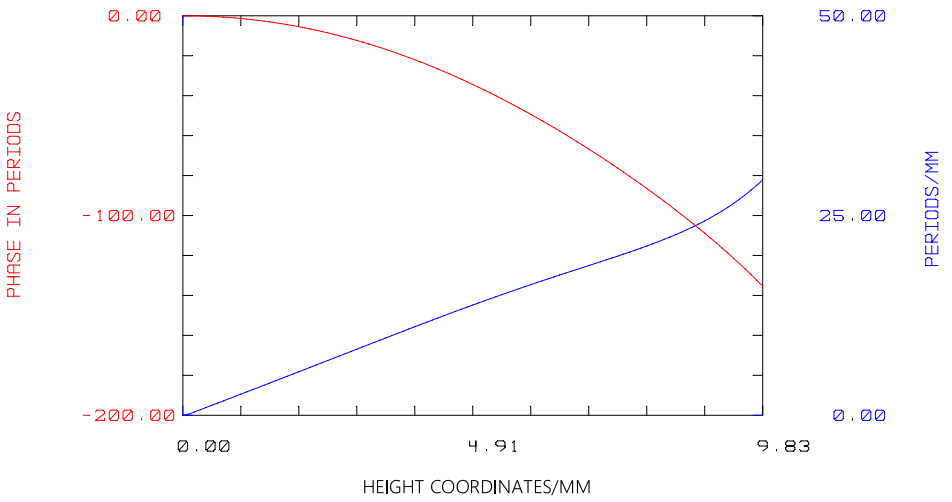

Fig. 8 Phase plot of the DOE surface

Table 3 Prescription of the fisheye lens

Surf.	Radius (mm)	Thickness (mm)	Glass
Object	Infinity	Infinity	N-PSK53A
1 lens1	46.006	13.495	
2	11.608	8.610	
3 lens2	26.134	1.514	N-LAK34
4 ASP	7.153	4.484	
5 lens3	26.509	3.581	SF5
6	− 707.273	0.019	
7STO	Infinity	0.747	
8 lens4	− 77.958	7.679	N-SK5
9 ASP	− 10.009	2.327	
10 lens5	928.888	7.324	N-PSK57
11 ADOE	− 9.122	1.199	SF57
12	− 19.731	19.342	
13 lens7	Infinity	1.204	PK1
14	Infinity	1.168	
IMA	Infinity		

Table 4 Aspheric coefficient

Surf.	4	9	11
k	0.0962	0.1156	− 0.2455
α_1	-1.0668×10^{-2}	3.5284×10^{-3}	9.3686×10^{-3}
α_2	-2.1620×10^{-5}	9.2910×10^{-5}	3.0116×10^{-5}
α_3	-1.1090×10^{-6}	9.8380×10^{-8}	-1.003×10^{-7}
α_4	1.3883×10^{-8}	1.8865×10^{-8}	1.3056×10^{-9}

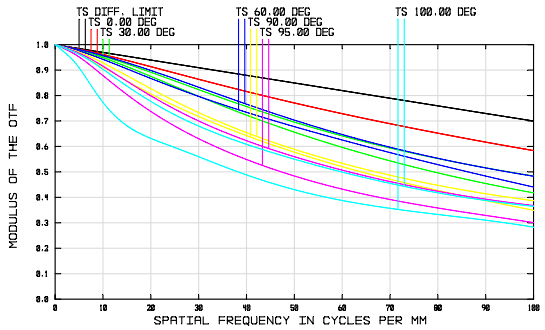

Fig. 9 MTF of the fisheye lens

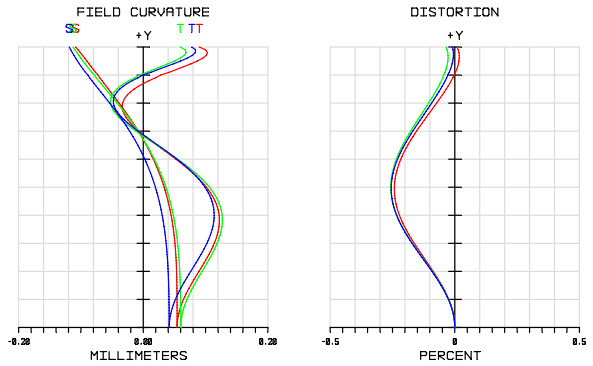

Fig. 10 Field curvature and distortion plot

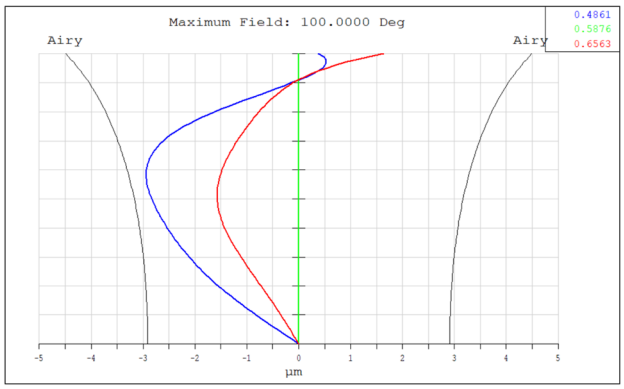

Fig. 11 Lateral color plot of the fisheye lens

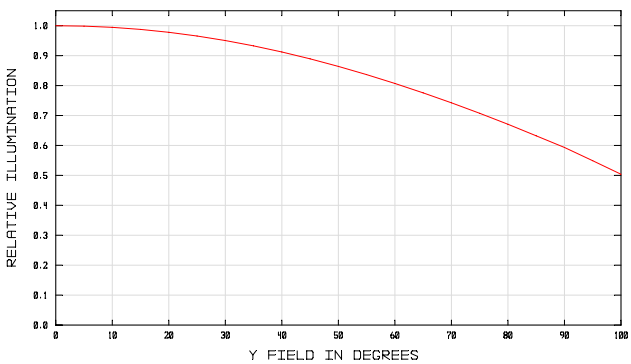

Fig. 12 Relative illumination of the fisheye lens

aberrations for 0.707 FOV compensate each other to make the field curvature aberrations close to zero. "T" represents the tangential field curvature and "S" represents the sagittal field curvature. As shown in Fig. 10, the field curvature values of "S" and "T" are close to zero for 0.707 FOV, and the values are equal for 0 FOV. Therefore, the first-order and higher-order astigmatism aberrations were corrected to zero for 0.707 and 0 FOVs.

The maximum barrel distortion was − 0.25% for the whole image. Figure 11 shows an excellent lateral color aberration curve. The chromatic aberration is under the airy disk radius. As shown in Fig. 12, the relative illumination decreases monotonically with the design angle of field and the value of the edge field (100°) is above 50%.

The performance evaluation of the fisheye lens satisfied its design requirements.

Table 5 shows the results of the performance comparison of the ADOE fisheye lens with a patented (EP2637056A1) fisheye lens. The imaging diameter for the ADOE lens is 1.5 times larger. Further, if the pixel size of CCD is 5.2 µm, the resolution of the ADOE lens is higher by about 30 MPx, which effectively improved the resolution of the imaging system. By contrast, other imaging performances improved significantly.

4.3 Tolerance analysis

The lens performance of ultrahigh-resolution and wide FOV is very sensitive to manufacturing and fabrication tolerance. Therefore, it is necessary to search for rational tolerance to balance both image quality and processing requirements. As per the evaluation criterion, the average value of MTF should be 0.45 at 100 lp/mm. The tolerance analysis of the fisheye lens—using ZEMAX—is presented in Table 6. The radius tolerance of sixth surface, the element decenter of the cemented lens, and the index tolerance are the main factors for the reduction of the MTF values. To perform an overall assessment of lens tolerance, we used 20 cycles of Monte Carlo simulations in the normal distribution. At this point, the average MTF was 0.236, and 90% of average the MTF values for Monte Carlo lens were above 0.25 at 100 lp/mm.

4.3.1 Distortion image calibration

The omnidirectional gaze photoelectric imaging system can catch hemispherical or ultra-hemispherical space scenery, which can cause a large barrel distortion. The distortion curve of the optical system (Fig. 13) was fitted using a polynomial function—described in Eq. (21)—to express the relationship between the real height (r') and the ideal height (r) of the image surface, which is shown in the Eq. (21).

$$r' = p_1 \times r^6 + p_2 \times r^5 + p_3 \times r^4 + p_4 \times r^3 + p_5 \times r^2 + p_6 \times r + p_7 \tag{21}$$

Table 6 Tolerance result of the ultrahigh resolution fisheye lens

Parameter	Surf.	Value
Radius (fringes)	S1–S5, S7, S9–S14	± 5
	S6, S8	± 4
Thickness (mm)	S1, S5, S6, S8, S9, S11, S12, S13	± 0.05
	S2, S3, S4, S7, S10	± 0.03
Element decenter (mm)	All	± 0.03
Element tilt (°)	All	± 0.01
Surface decenter (mm)	All	± 0.03
Surface tilt (°)	S1, S2, S3, S10, S12	± 0.03
	S5, S6, S8	± 0.01
Refractive index	All	± 0.0001
Abbe number (%)	S1, S3, S8, S10	± 0.1
	S5, S11	± 0.08

where r' is the real imaging height, r is the ideal imaging height, and the relationship between r and r' using the calculated distortion curve coefficients is shown in Fig. 13. The curve coefficients are shown in Table 7.

The following Eqs. (22) and (23) show the coordinate transformation of the real and deal images. (u, v) are the point coordinates of the distorted image, and (x, y) are the point coordinates of the distortion-free image. When r is 0 in the center point of the image, the system has no distortion. The data of the designed lens are read into an optical design software CODE V to simulate the distorted image shown in Fig. 14 (left). Using the model described in Eqs. (22) and (23), and the fitting coefficients in Table 7, the image without distortion (Fig. 14, right) was obtained from the calculations by CODE V.

$$\begin{cases} x^2 + y^2 = r^2 \\ u = xr'/r \quad r > 0 \\ v = yr'/r \end{cases} \tag{22}$$

Table 5 Performance comparison of patent EP2637056A1 and ADOE fisheye lens

Performance	EP2637056 A1	ADOE fisheye lens	comparison
Focal length (mm)	10.33	11.6	Conform to specifications
Field of view	180°	200°	Increased by 20°
Imaging diameter(mm)	28.26	40.3	Increased 1.5 times
Average MTF value	0.142	0.389	Upgraded 2.7 times
Minimum MTF value	0.048	0.292	Upgraded 6 times
Maximum *F*-Theta distortion	− 12.6%	− 0.25%	Decreased 50 times
Maximum Lateral color aberration (µm)	18.44	1.83	Decreased 10 times
Maximum RMS radius (90°)	67.08	11.01	Decreased 6 times
Minimum relative illumination	0.89	0.51	Decreased 0.38 times

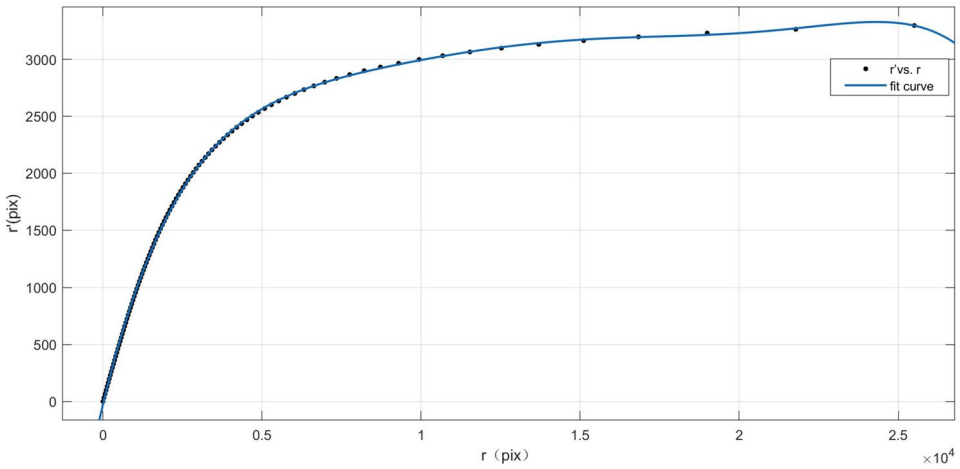

Fig. 13 Fitting curve of actual image height r' and ideal image height r

Table 7 Curve coefficients

Coefficient	p_1	p_2	p_3	p_4	p_5	p_6	p_7
Value	− 3.577e−22	3.164e−17	− 1.119e−12	2.038e−08	− 2.055e−04	1.158	− 28.5

Fig. 14 Omnidirectional gaze image calibration. Left part shows a distorted image and the right is the image without distortion

$$\begin{cases} u = x \\ v = y \end{cases} \quad r{=}0 \tag{23}$$

5 Conclusions

In this study, we proposed a new method for the design of an omnidirectional gaze optical image system with ultrahigh-resolution and long focus. An ADOE surface was used to reduce the number of elements and correct the off-axis aberration. As a result, the system was realized for a sensor of 80 MPx count with an FOV of 200° × 360° and an EFFL of 11.6 mm. The F/# of the system, total length, and maximum diameter of the elements were 4, 73 mm, and 74 mm, respectively. The MTF of the center field was above 0.6 and marginal field was better than 0.3 at 100 lp/mm frequency in the whole range of visible-light wavelength. Overall, it provides a good method to design an omnidirectional gaze optical imaging system with an ultrahigh-resolution.

References

1. Wang, Y. Z.: Fisheye Lens. China Science Publishing& Media Ltd, pp. 1–64 (1985)
2. Samy, A.M., Gao, Z.S.: Simplified compact fisheye lens challenges and design. J. Opt. **44**(4), 409–416 (2015)
3. Pernechele, C.: Hyper hemispheric lens. Opt. Express **24**(5), 5014–5019 (2016)

4. Alshomrany, A., Clark, N.A.: Fisheye lens conoscopy. Liq. Cryst. **42**(3), 271–287 (2015)
5. Hao, X., Kuang, C., Gu, Z., et al.: From microscopy to nanoscopy via visible light. Light-Sci Appl **2**(10), e108 (2013)
6. Wu, Q., Turpin, J.P., Werner, D.H.: Integrated photonic systems based on transformation optics enabled gradient index devices. Light-Sci. Appl. **1**(11), e38 (2012)
7. Mizuguchi, K.: Fisheye lens. U. S. Patent. No. 6,844,991 B2, 1–20 (2005)
8. Mizuguchi, K.: Fisheye lens. U. S. Patent. No. 7,161,746 B2, 1–20 (2007)
9. Thibault, S., Parent, J., Zhang, H., Roulet, P.: Design, fabrication and test of miniature plastic panomorph lenses with 180° field of view. Proc. SPIE **9293**, 92931N-1–92931N10 (2014)
10. Myles, A., Zorin, D.: Controlled-distortion constrained global parametrization. Acm Trans. Gr. **32**(4), 1–13 (2013)
11. Samy, A.M., Gao, Z.S.: Fovea-stereographic: a projection function for ultra-wide-angle cameras. Opt. Eng. **54**(4), 45104-1-8 (2015)
12. Samy, A.M., Gao, Z.S.: Foveated fisheye lens design using an angle-variant distortion projection function. Opt. Rev. **22**, 919–927 (2015)
13. Wang, Z.J.: Theoretical Foundation of Optical Design. Science, pp. 455–458 (1985)
14. Ma, T., et al.: Design of a freeform varifocal panoramic optical system with specified annular center of field of view. Opt. Express. **19**(5), 3843–3853 (2011)
15. Heu, M.: Fisheye lens. EP. No. 2,637,056 A1, 1–20 (2013)
16. Wu, D.X., Li, G., Wang, B., et al.: Fabrication of microstructured surfaces by five-axis ultra precision machine tool. Key Eng. Mater. **625**, 187–191 (2014)
17. Zhao, L.D.: Studies on design theory and application of multilayer diffractive optics. Changchun Univ. Sci. Technol. **D**, 20–25 (2019)